The definitive publisher version is available online at https://doi.org/10.1016/j.jclepro.2022.135121

Efficient Extraction of Silica from Openly Burned Rice Husk Ash as Adsorbent for Dye Removal

Jahid Bin Haider[a], Md. Irfanul Haque[a], Mozammel Hoque[b], Md. Mosaddek Hossen[a], M. Mottakin[a], Abdul Khaleque[a], MAH Johir[c], John L. Zhou[c], Mohammad Boshir Ahmedc[c, d*], Masoumeh Zargar[e].

[a]*Department of Applied Chemistry and Chemical Engineering, Bangabandhu Sheikh Mujibur Rahman Science and Technology University, Gopalganj-8100, Bangladesh*

[b]*Department of Applied Chemistry and Chemical Engineering, University of Rajshahi, Rajshahi 6205, Bangladesh*

[c]*Centre for Green Technology, School of Civil and Environmental Engineering, University of Technology Sydney, 15 Broadway, NSW 2007, Australia*

[d]*School of Materials Science and Engineering, Gwangju Institute of Science and Technology, Buk-gu, Gwanjgju-61005, South Korea*

[e]*School of Engineering, Edith Cowan University, Joondalup, WA 6027, Australia*

Corresponding author:
Dr Mohammad Boshir Ahmed
Mohammad.Ahmed@gist.ac.kr

Abstract:
Rice is the staple food in many countries including Bangladesh. In Bangladesh, >80% of the total irrigated area is planted with rice. This leads to generate a huge amount of rice husk (RH) as a solid waste which requires proper management. This study, therefore, aimed to extract amorphous silica from openly burned rice husk ash (RHA) using a low-cost energy-saving method by avoiding calcination or combustion processes. The extracted silica was then applied for the removal of environmental contaminants i.e., methylene blue dye from an aqueous solution. It was found that the yield of silica produced from sulfuric acid-pretreated RHA was 72.4%. The FTIR absorption peaks in 1057 and 783 cm^{-1} indicate the presence of a highly condensed silica-containing asymmetric and symmetric siloxane (Si-O-Si) network mixture. The broad maximum bond peak intensity at $2\theta = 22°$ by x-ray diffraction analysis also indicates that the produced silica was amorphous with a mesoporous structure. The sulfuric acid treated RHA-based silica surface area was 182 m^2/g. This silica resulted in a maximum adsorption capacity of 107 mg/g of methylene blue at pH 8 with a faster equilibrium of 60 minutes. The mechanistic study indicated that Langmuir's and Freundlich both adsorption isotherms were fitted well which indicated homogeneous adsorbent surfaces involving monolayer and multilayer adsorption processes.

Keywords: Rice husk ash; Acid-pretreatment; Mesoporous silica; Methylene blue; Adsorption

1. Introduction

Bangladesh is an agricultural country, and approximately 80% of the total irrigated lands are used for rice production (BRRI, 2021). Consequently, the rice processing industries produce large amounts of rice husk waste. The milling of paddy rice generates about 70% yield of rice as the principal product together with unconsumed portions of rice husk (RH, 20%), rice bran **(**8%), and rice germ (2%) (Me and Bee Ling, 2016; Van Hoed et al., 2006). As significant amounts of RH are produced during the milling of paddy rice, RH has been utilized for different purposes including activated carbon production (He et al., 2021; Wazir et al., 2020), electricity generation (Ejiofor et al., 2020; Silva et al., 2021), nitrates, and heavy metal removal from wastewater (Ag et al., 2018; Sadeghi Afjeh et al., 2020). However, most RH in Bangladesh is being utilized for energy production. Hence, a significant amount of rice husk ash (RHA) is generated by those small-scale industries enriched with a high portion of silica content (Zareihassangheshlaghi et al., 2020). The silica content in RHA depends on various factors including climate, soil types, harvesting season, the amounts of fertilizers used during cultivation, and geographical and environmental aspects (Beidaghy Dizaji et al., 2019; Singh et al., 2022). This RHA is often dumped on land leading to pollution of the soil environment. Therefore, recycling of such RHA into valuable products or use as adsorbent (Silvalingam and Sen, 2020; Costa and Paranhos, 2019; Mor et al., 2016; Lakshmi et al., 2009; Mane et al., 2007) has great demand as RHA contains more than 90% silica with small fractions of other inorganic oxides such as sodium, potassium, iron, and magnesium (Alam et al., 2020). Among these constituents, silica is the crucial element forming the inorganic compound silicon dioxide (SiO_2). Although silica is found in nature, mainly as sand or sand quartz, RHA represents another potential source. Silica is industrially used for many purposes e.g., as an additive for catalyst, insulation, toothpaste, coating solutions, and cosmetics (Park et al., 2021).

Furthermore, rice husk-derived silica is used as an adsorbent for organic dye removal (Niculescu and Raboaca, 2021), for the removal of phosphates and heavy metals (Dutta Gupta et al., 2021; Suzaimi et al., 2020), filler in plastics and rubber compounding (Karthigairajan et al., 2020), wastewater treatment (Mohamed and Alfalous, 2020), gas purification (Bakdash et al., 2020), ceramics processing (Sobrosa et al., 2017), thermal insulators (Hossain et al., 2017; Sembiring et al., 2016), concrete (Zareei et al., 2017), steel, and refractory bricks (Shen, 2017).

Recently, several studies suggested that pure silica can be effectively extracted from RHA through a combination of extraction and purification methods such as alkali leaching (Ma et al., 2012), acid leaching (Sankar et al., 2016; Schliermann et al., 2018) and thermal treatment (Bakar et al., 2016; Beidaghy Dizaji et al. 2022a; Beidaghy Dizaji et al., 2022b). Singh et al., (2022) reported that if rice husk is calcined below 900℃, then amorphous silica is produced; whereas if calcination temperature rises above 900℃, crystalline silica is produced. Chun et al., (2020) burned RHA at 900℃ for 12 h after sulfuric acid pretreatment to produce ordered mesoporous nano-silica particles with 5.0 M NaOH. Azat et al., (2019) produced 98.7% pure silica with 625 m^2/g surface area from RHA by leaching with 2.0 M NaOH at 90℃ for 2 h. 89% silica yield was found with two-stage continuous processes and 79% with a single-stage when RHA was treated with 0.2 M NaOH at 80℃ for 3 h (Park et al., 2021). After extraction, the precipitate was calcined at 900℃ for 6 h to produce 98.5% pure silica with a surface area of 1.973 m^2/g. Another study reported a 91% yield with 93% purity of silica obtained from RHA with 1.0 M NaOH for 1 h (Kalapathy et al., 2000). They used 660℃ temperatures for 8 h to convert rice husk to ash. Similarly, Ma et al., (2012) prepared silica powder when RHA collected from a power plant was heated at 120℃ with 4.0 M NH_4F for 3 h with a conversion yield of 94.6%. Therefore, all processes used pre-calcination or post-calcination techniques to extract and purify silica from RHA.

Literature shows that controlled burning or calcination processes were carried out by changing the temperature (post calcination) as well as the use of alkali before or after extraction. Therefore, this study aims to extract silica from RHA via a non-post calcination or carbonization method by collecting the RHA from a local rice processing mill. This process leads to the low-cost and less energy-intensive and sustainable production of pure silica from RHA. In addition, the extracted silica was then applied as a natural adsorbent to remove organic pollutants such as methylene blue dye from the aqueous solution.

2. Materials and Methods

2.1. Materials

Rice husk ash (RHA) was collected from the Tungipara Rice Processing Mill, Gopalganj, Bangladesh. All the reagents used in this study were of analytical grade. Sulfuric acid (98%) and sodium hydroxide pellets were purchased from Merck Specialties Private Limited, India.

2.2. Pretreatment of RHA

Incompletely burned RHA is separated using a 45-mesh sieve, and there present no visible slag in the collected sample. After sieving, half of the total ash was washed using water, and another half was washed with 0.5N H_2SO_4 acid with constant stirring at 40°C. A magnetic stirrer hotplate (Scilogex Magnetic Stirrer with hot plate, model MS7-H550-Pro, USA) was used for heating and stirring. After acid washing, RHA samples were neutralized to pH 7 by washing them with distilled water. Washed samples were dried at 80°C for 12 h, and stored in zip-lock bags at room temperature (**Figure 1**). Silica produced from water-washed RHA was denoted as WW_RHA, and silica produced from acid-washed RHA was denoted as AW_RHA.

2.3. Silica preparation from RHA

Pretreated RHA was leached at a constant temperature (105°C) and varying the time from 0.5 h to 3.0 h in the presence of 3.0 M NaOH. To do so, 5 g ash was weighed and placed in a flat-bottomed flask with 100 ml 3 M NaOH. At the end of the experiments, the sodium silicate and leachate solution were separated from insoluble residue using Whatman filter paper 125 mm Grade-1. Then the separated solution was neutralized to pH 7 with 3 M H_2SO_4 solution with continuous stirring, and allowed to stand overnight to precipitate silicic acid (**Figure 1**). The precipitated product was collected and washed thoroughly with distilled water to remove any unwanted water-soluble salt and clouds of dust. After washing, the final product was dried at 80°C for 24 h for converting silicic acid to pure silica; and stored in an airtight sample holder for further use.

"Figure 1"

2.4. Characterizations of silica

The surface morphology of produced silica was observed by employing field emission scanning electron microscopy (FESEM, JSM-7610F, JEOL, Japan). Energy dispersive spectroscopy (EDS; 7610F, JEOL, Japan) coupled with FESEM was used to identify the presence of corresponding elements in silica samples. SEM-EDS analysis was performed under a low-pressure vacuum with a processing time of 3.25 s, beam accelerating voltage of 15 kV at beam aperture of 6 mm, with a working distance of 7.6 mm, magnification of 2000, probe current of 1.0 nA, and EDX count rate at 1400 ± 200 cps. X-ray fluorescence (XRF) was done using SHIMADZU ED-XRF (EDX-8000, Japan) to determine the chemical compositions of the initial RHA and

Rigaku WD-XRF (ZSX Primus IV, Japan) to determine the chemical compositions of the produced silica. XRF was done taking a 0.2 g sample, pressing pressure of 10 lb, and 3 minutes of palletization time. X-ray diffraction (XRD) patterns of silica from WW_RHA and silica from AW_RHA were recorded using Rigaku AC 2021 (Japan) X-Ray diffractometer using Kβ filter 1D for Cu and HyPix-400 (horizontal) detector operated at 50 mA and 40 kV at a scan rate of 20 °/min in the 2θ range of 5-30°. FTIR spectra identified the functional groups present in SiO_2 precipitate. An IR Prestige 21 FTIR (SHIMADZU, Japan) spectrometer was used with the ATR technique at a spectral range from 700 to 1400 cm^{-1} for 30 scans at a speed of 4 cms^{-1}. The Brunauer-Emmett-Teller (BET) surface area of silica was determined from N_2 adsorption measurements using BET-201-A Sorptometer (PMI, USA). N_2 adsorption/desorption isotherms were recorded in the range of relative pressures, P/P_0, from 0.0 to 0.977. To remove any moisture or adsorbed contaminants, samples were outgassed to 20 microns vacuum overnight at 120℃ before measurements.

2.5. Adsorption of organic dye using extracted silica

The stock solution of methylene blue (MB) was prepared with distilled water. Firstly, we studied the effect of pH on dye adsorption. To do so, the pH was adjusted from 2 to 12, using 0.1 M HCl and 0.1 M NaOH solutions at room temperature before adsorption experiments were carried out for 6 h to determine sorption capacity at equilibrium. HI-2211 Bench-type pH meter was used for measuring the pH of the solution. Before measuring the pH of the solution, the pH meter was calibrated using buffer solutions of pH 4 and 7 (BDH). The effect of pH on adsorption was studied for both acid-washed and water-washed silica. The absorbance of each test solution was measured before and after performing the adsorption at 660 nm using T 92+ Double Beam UV-Vis Spectrophotometer (PG Instrument, UK). Then we carried out the kinetics experiment to determine the equilibrium time of adsorption for both acid-washed and water-washed silica. The

kinetics studies were carried out for up to 240 minutes. For each type of silica, the initial concentration of MB was 1000 mg/L, and the adsorbent amount was 0.25 g. Starting from 5 minutes, the sample was taken at regular intervals, and absorbance was measured to determine the equilibrium concentration and amount adsorbed at equilibrium. The adsorption process reached an equilibrium around 60 minutes. The pseudo-first-order (PFO) kinetic model (equation 1) and the pseudo-second-order (PSO) (equation 2) were fitted to the experimental data.

$$\text{PFO: } Q_1 = Q_e\,(1 - e^{-K_1 t}) \quad \ldots\ldots\ldots\ldots\ldots (1)$$

$$\text{PSO: } Q_2 = \frac{K_2 {Q_e}^2 t}{1 + K_2 {Q_e}^2 t} \quad \ldots\ldots\ldots\ldots\ldots (2)$$

where Q_e (mg/g) is the adsorption amount at equilibrium, and K_1 (min^{-1}) and K_2 ($mg^{-1}min^{-1}$) are PFO and PSO kinetic rate constant, respectively. These parameters were estimated by nonlinear regression weighted by the dependent variables.

Then adsorption isotherm experiments were conducted by adding 0.25 g of silica to 100 ml of MB solution in a conical flask. The initial concentrations of MB were kept within 100 to 500 mg/L. The mixtures were kept at room temperature with constant stirring for 60 minutes at pH 8 (as higher adsorption capacity was found at this pH). Two standard sorption models called Langmuir and Freundlich isotherm models were used to fit the experimental data.

The apparent sorption distribution coefficient (K_d, L/kg) is defined as the ratio of adsorbate sorbed per unit sorbent mass (Q_e, mg/g) to adsorbate concentration in solution (C_e, mg/L) at equilibrium and was calculated using Eq. (3):

$$K_d = 1000\,\frac{Q_e}{C_e} = 1000\,\frac{V}{M}\left(\frac{C_0 - C_e}{C_e}\right) \quad \ldots\ldots\ldots\ldots\ldots (3)$$

where V is the solution volume (L), C_o is the initial adsorbate concentration in water (mg/L), and M (g) is the sorbent mass. The Langmuir and Freundlich isotherm models can be represented as follows:

$$\text{Freundlich model: } Q_e = K_F C_e^{1/n} \quad \ldots\ldots\ldots\ldots\ldots (4)$$

$$\text{Langmuir model: } Q_e = \frac{Q_{max} K_L C_e}{1 + K_L C_e} \quad \ldots\ldots\ldots\ldots\ldots (5)$$

where Q_{max} is the maximum adsorption capacity (mg/gm), K_F is the Freundlich capacity-affinity coefficient ($mg^{1-n}L^n g^{-1}$), 1/n is a dimensionless number related to surface heterogeneity, and K_L is the Langmuir fitting parameter (Lmg^{-1}). Parameters were estimated using the above equations and fitting in Origin pro software by nonlinear regression weighted by the dependent variable.

3. Results and discussion

3.1. Mechanism of silica extraction from RHA

The silica production process from RHA involves two steps (Chun and Lee, 2020). Firstly, the leaching of silica from RHA to the solution, and secondly, silica precipitation. Previous studies indicate that amorphous silica is soluble in an alkaline medium when pH was increased above pH 9 (Alexander et al., 1954). As the average process temperature for the production of RHA in the rice processing mill is below 650°C, therefore according to the literature it contained mainly amorphous silica. When RHA is treated with NaOH solution, silica from RHA dissolves by forming Na_2SiO_3 according to the following chemical reaction 6:

$$2NaOH + SiO_2(ash) \rightarrow Na_2SiO_3 + H_2O \quad \ldots\ldots\ldots\ldots\ldots (6)$$

The solubility of silica increases with the increase in pH; therefore, lowering the pH or neutralizing the alkaline silicate solution is the essential requirement for precipitating silica from the solution. Sulfuric acid is a standard method for neutralizing the sodium silicate solution for silica precipitation (Soltani et al., 2015). Following reaction-7 involves this process:

$$Na_2SiO_3 + H_2SO_4 \rightarrow SiO_2 \downarrow + Na_2SO_4 + H_2O \quad \ldots\ldots\ldots\ldots\ldots (7)$$

3.2. Chemical composition of initial RHA

The chemical composition of the initial RHA and extracted silica was examined by Energy Dispersive X-ray Fluorescence (ED-XRF) spectroscopic measurement. The RHA used in this study contains: SiO_2 (90.990%), Al_2O_3 (3.982%), K_2O (1.864%), CaO (1.811%), Fe_2O_3 (0.496%), SO_3 (0.307%), Cl (0.302%), MgO (0.140%), and ZnO (0.029%); and it undergoes 3.103% weight loss on ignition. The results from ED-XRF analysis (**Table 1**) show that SiO_2 was the main component of the siliceous precipitate, and the contents of various metal oxide impurities were low. In our case, the purity of silica produced from RHA by avoiding calcination was 96.3% and 94.0% for silica from WW_RHA and silica from AW_RHA, respectively. The obtained silica masses were 94-96.3% for silica extracted via acid and water washed. It is noticeable that although pre-carbonization or post-carbonization was not used, our results showed a higher amount of silica present in the final composition. Whereas, many studies of silica extraction from RHA were carried out using pre- or post-calcination methods involving high temperature (above 600°C), with a slightly better percentage of silica content in the final products (i.e., 93-98%) (Azat et al., 2019; Bakar et al., 2016; Chun et al., 2020). For example, Park et al., (2021) obtained 98.5% silica from RHA, but they calcined their samples after the extraction process to obtain the final product. More comparison is listed in **Table 1**. In contrast, we used RHA produced from burning rice husk in an open environment to heat the boiler in local rice processing mills and avoid further calcination

steps before or after the extraction process. Therefore, our process significantly reduces the cost of silica production by avoiding further calcination. In addition, the presence of other metallic oxides was minimal in quantities. The result shows no Na_2O present in the initial RHA but presents ~1.78-3.09% of Na_2O in the final product. This might come as a precipitant from the NaOH solution, and can be reduced by applying stringent washing steps (Park et al., 2021).

"Table 1"

3.3. SEM and EDS analysis of produced silica

The surface morphology of the produced silica was observed by scanning electron microscopy (SEM) and shown in **Figures 2a and 2b**. The results show that WW_RHA silica appears to be more porous with a rough surface (**Figure 2a**), whereas AW_RHA surface is more uniform with a well-distributed structure (**Figure 2b**). Energy dispersive spectroscopy (EDS) analysis showed that oxygen element was more abundant for AW_RHA compared to WW_RHA, and silicon composition was lower for AW_RHA (**Figure 2c**). These eventually resulted in lower content of silica in AW_RHA compared to WW_RHA (**Figure 2d**). In addition, EDS results showed a similar profile as obtained by XRF studies.

"Figure 2"

3.4. Effect of time on the extraction of silica from RHA

The percentage yield of the produced silica from the hydrolysis of RHA is plotted graphically (**Figure 3a**). The results show that the yield percentage of produced silica increased with the

increase in dissolution time up to 2 h for both water-washed and sulfuric acid-washed RHA. Over 2 h of reaction time, the percentage yield does not increase significantly. The yield percentage of silica produced from water-washed and acid-washed RHA was 71.71% and 72.44%, respectively for 2 h reaction time and without further calcination. Therefore, the optimum time of silica extraction from RHA was 2 h at 105℃ by using 3.0 M NaOH solution and constant stirring. On the other hand, Park et al., (2021) reported 79.9% silica yield by using 0.5 M NaOH for 3 h reaction time in 80℃, but they calcined the precipitated silica at 900℃ for 6 h for the final product. Similarly, Azat et al., (2019) extracted silica from RHA after 2 h of reaction time with 2 M NaOH at 90℃, but they calcined the sample at 600℃ before alkali extraction. Therefore, our method of silica extraction from RHA involves lower energy consumption than other methods.

3.5. FTIR analysis of produced silica

Figure 3(b) presents the FTIR-ATR spectra to identify functional groups of produced SiO_2 from RHA data between 700 to 1400 cm^{-1} for silica from WW_RHA and silica from AW_RHA. The literature shows that the absorption band for SiO_2 is known to be within the wavenumber range of 1000-1100 cm^{-1} (Post et al., 2018). The IR spectra at the ranges 778-799 and 1035-1125 cm^{-1} could be attributed to stretching, and asymmetrical stretching vibration of Si-O-Si (Prempeh et al., 2021). For example, Melendez et al., (2014) reported Si-O-Si stretching and bending vibration peaks at 1058 cm^{-1} and 800 cm^{-1}. RHA-derived amorphous silica shows absorption stretching vibration peaks at 1055 cm^{-1} (Azat et al., 2019); and 1051 cm^{-1} (Umeda and Kondoh, 2010). Widjonarko and Kartini (2014), found the presence of both asymmetric siloxane (Si-O-Si) and symmetric siloxane (Si-O-Si) in pure silica gel, confirmed by FTIR absorption peaks at 1087 cm^{-1} and 802 cm^{-1}, respectively. Singh et al., (2022) found the symmetric and asymmetric stretching vibration of the Si-O-Si bond at 794 cm^{-1} and 1109 cm^{-1} for amorphous silica

nanoparticles. **Figure 3(b)** shows the absorption peaks in this study are found at 1057 cm^{-1} and 783 cm^{-1} for silica from WW_RHA; and 1053 cm^{-1} and 802 cm^{-1} for silica from AW_RHA, respectively. These peaks indicate a highly condensed silica network containing mainly asymmetric siloxane (Si-O-Si) together with some symmetric siloxane (Si-O-Si) in the produced silica from RHA without calcination. Due to removing acid-soluble impurities, silica from AW_RHA possesses much higher absorbance than silica from WW_RHA in the asymmetric siloxane region, where both possess approximately the same absorbance in the symmetric siloxane region. Therefore, it is clear that acid pretreatment affects mainly the asymmetric siloxane network in silica.

"Figure 3"

3.6. XRD analysis of produced silica

The crystallinity of produced silica from WW_RHA and silica from AW_RHA was investigated using XRD spectra, and corresponding data were plotted in **Figure 3(c)**. Beidaghy Dizaji et al. (2019) summarized that the crystallization temperature shifts to higher values from 600℃ to about 1000℃ when RHA is pretreated with different chemicals. The removal of alkali metal content in pre-treatment is the reason for this shift. Azat et al., (2019) found a broad diffused peak in XRD with a maximum intensity at $2\theta=22^{o}$ with the corresponding d-spacing value of 0.36 nm which confirmed the amorphous nature of produced silica from RHA when calcined at 600℃. Park et al., (2021) found broad diffraction at $2\theta=20^{o}$ for RH-derived silica while calcined at 900℃. In this study, without any calcination, we found broad diffused peaks with a maximum intensity at $2\theta = 21.7°$ for silica from WW_RHA, and at $2\theta=22^{o}$ for silica from AW_RHA, respectively.

These broad peaks indicate the amorphous nature of the produced silica and confirm the absence of any crystalline silica. However, the peak for WA_RHA is slightly sharper than the peak for silica from WW_RHA. This was due to sulfuric acid pretreatment before leaching with NaOH which removed organic compounds from the RHA. Therefore, without post calcination, our extracted silica gives similar peaks as reported in other studies.

3.7. Nitrogen adsorption isotherms and BET surface areas

The nitrogen adsorption-desorption isotherms for silica from WW_RHA and AW_RHA are shown in **Figures 3(d) and 3(e)**. The isotherms of silica produced from untreated and acid pretreated RHA are closer to type III isotherms, similar to the isotherms derived by Azat et al. (2019). The results were almost similar to the findings of Beidaghy Dizaji et al., (2022) and Singh et al., (2022). They found that the porosity of silica-rich ashes diminishes, once the crystallinity fraction is higher than 10 wt.%. The results show that N_2 adsorption on silica from AW_RHA is higher than on silica from WW_RHA; which is supported by the BET surface area and pore volume data. The weak hysteresis loop and curvature in low pressures indicate a mixture of mesoporous-macroporous materials. It indicates the formation of monolayers, bilayers, trilayers, and so on at the same time, resulting in an almost exponential increase in the amount of adsorption.

The Brunauer-Emmett-Teller (BET) specific surface area of silica was determined from N_2 adsorption-desorption measurements and pore volume and pore diameter (pore size distribution) were calculated using Pierce and Barret-Joyner-Halenda (BJH) desorption methods. The specific surface area, pore volume, and average pore diameter of the produced silica from RHA are shown in **Table 2** and **Figure 3f**. The R^2 of BET transfer plots are 0.9998 and 0.9997, and the BET C values are 154.45 and 142.91 for AW_RHA silica and WW_RHA silica respectively. The BET surface area (182 m^2/g) found in this study was lower than that found by Bakar et al., (2016), but

higher than that found (88 m^2/g) by Chun et al., (2020) for RHA-derived silica. Bakar et al., calcined RHA at 600°C, and Chun et al., calcined RHA at 900°C before silica extraction. We found a higher surface area than Chun's study, though we avoided calcination. More comparison is listed in **Table 2**. However, the BET surface area and pore volume of silica from AW_RHA are higher than silica from WW_RHA. This higher value in AW_RHA is supported by Beidaghy Dizaji et al., (2021). They mentioned that at a lower temperature (<900°C), BET surface area is influenced by the chemical pre-treatment and high when acid is used for pre-treatment. The hydrolysis of any organic compounds present in small quantities in RHA is the reason for this increase in surface area for silica from AW_RHA. Therefore, highly porous SiO_2 is found when pretreated with sulfuric acid before silica extraction, supported by higher pore volume for silica from AW_RHA. The average pore diameter data indicates that silica produced from RHA is mesoporous. Therefore, sulfuric acid pretreatment slightly increased the surface area and pore volume and reduced the pore diameter.

"Table 2"

3.8. Mechanism and effect of pH on MB removal by RHA-derived silica

The solution pH affects the charge distribution of the adsorbent surface and the interactions between the adsorbent and the dye molecules. To determine the effect of pH on the K_d values for MB removal from aqueous solution by rice husk-derived silica, we studied the effect of pH ranging from 2 to 12 by taking 100 mg/L initial MB concentration at room temperature with 0.25 g adsorbent loading, and the results are depicted in **Figure 4(a)**.

"Figure 4"

The figure shows that the increase in pH from 2 to 8 caused a substantial increase in the K_d values for MB removal for both water-washed and acid-washed silica. The adsorbent surface became negative, which enhanced the adsorption of positively charged MB dye by electrostatic attraction force, which might cause these increased K_d values with increasing initial pH. But, after pH 8, the K_d values decreased with an increase in pH. Because above pH 8, the adsorbent surface will hold the more partial negative charge as O^- in **Figure 5.** So, a repulsive force arises between the adsorbent surface and the presence of a partial negative charge of chloride ions on MB. Therefore, pH 8 is chosen as the optimum pH for further study. Literature shows that with the modification of silica adsorbent surface, the optimum pH can be between 6.8 to 11 (Adam et al., 2013; Alver et al., 2020; Hongo et al., 2021; Sharma et al., 2010).

"Figure 5"

Adsorption of MB on silica surfaces can occur in three cases (**Figure 5**). In cases 1 and 2, electrostatic attraction between partially charged nitrogen-oxygen and partially charged sulfur-oxygen. Case 3 represents hydrogen bonding. In lower pH values, the adsorption occurs mainly by hydrogen bonding. These hydrogen bonds would be expected to occur between amino groups in the dye molecule and the silica surface hydroxyl groups. The surface becomes more ionic on the increasing pH value to neutral pH. Deprotonation starts when the cationic methylene blue reacts with the -OH group, eliminating HCl and increasing the adsorption capacity. This

mechanism is also supported by previous studies on pH-dependent data (Adam et al., 2013; Chandrasekhar and

Pramada, 2006; Hongo et al., 2021).

3.9. Adsorption kinetics for MB removal by RHA-derived silica

The contact time is an essential parameter for the dye adsorption process. The effect of time on MB removal by RHA-derived silica and corresponding PFO and PSO kinetics model fitting are shown in **Figure 4(b)**. It can be seen from the figure that the maximum uptake of MB reached maximum approximately in equilibrium time of 60 minutes for both water-washed and acid-washed RHA silica which is consistent with previous studies (Azevedo et al., 2017; Chen et al., 2012). Modifying RHA with alginate increased the equilibration time to 90 minutes (Alver et al., 2020). Singh et al., (2022) used UV-C irradiation with silica nanoparticles for the degradation of methylene blue dye, and they found ~100% of degradation within the initial 30 minutes of the adsorption onto silica-nanoparticles.

The nature of the adsorption process can be identified from the adsorption kinetics models. pseudo-first-order (PFO) and pseudo-second-order (PSO) models were used in this study to determine the adsorption process, and the calculated data were given in **Table 3**. The PFO and PSO kinetic models are well-fitted for both silica. Therefore, water-washed silica and acid-washed silica both followed PSO and PFO models indicating the role of the physisorption and the chemisorption processes (Agbovi and Wilson, 2021).

"Table 3"

3.10. Sorption isotherm for MB removal by RHA-derived silica

The Langmuir and Freundlich isotherms models were fitted for MB adsorption by RHA-derived silica. The sorption data were plotted in **Figure 4(c)** to find the best-fitted model, and corresponding data were given in **Table 4**. Figure and the corresponding R^2 values from table 4 indicate that sorption data were well fitted with both the Langmuir isotherm model and the Freundlich isotherm model. Fitting to the Langmuir isotherm means that RHA-derived silica has homogeneous adsorbent surfaces involving monolayer adsorption processes with similar adsorption sites whereas fitting to Freundlich isotherms indicated surfaces were multilayer coverings. Anyway, the Q_m values were in little agreement with the Q_e values (**Tables 3 and 4**). Previous studies of MB adsorption by RHA have found similar characteristics (Chen et al., 2012; Hongo et al., 2021), but if RHA is modified with alginate, it is better fitted with Freundlich isotherm (Alver et al., 2020).

"Table 4"

We further then calculated the sorption distribution coefficient K_d values. The K_d values decreased with the increase in MB concentration and were plotted with the equilibrium MB concentration in **Figure 4(d).** The observed values of Q_m and K_f for MB for both cases were higher than the values reported by Chen et al., (2012), Moeinian and Mehdinia (2019), and Hongo et al., (2021). Q_m and K_f values were lower than reported by Peres et al., (2018) and Chandrasekhar and Pramada (2006), who both used RHA directly without separating the silica. Therefore, there may also be many carbon-containing compounds that adsorb MB molecules.

4. Conclusions

This study reported a low-cost method for extracting silica from RHA, with > 94% pure mesoporous amorphous silica and a high yield conversion of > 72.3% without further calcination. XRF and FTIR results show that SiO_2 is the major component of the siliceous precipitate with a highly condensed siloxane (Si-O-Si) network structure with a surface area ranging from 165 m^2/g to 183 m^2/g. Adsorption studies showed that 107 mg of methylene blue can be adsorbed by 1.0 g of silica produced from acid-washed RHA at pH 8 within 60 minutes. Therefore, the results demonstrate the feasibility of environment-friendly extraction of silica from RHA with a high adsorption capacity for methylene blue. This research has proved the conversion of a waste material (i.e. RHA) to a valuable product (i.e. silica) as a natural element and effective adsorbent of contaminants. As a result, this method can prevent the dumping of RHA on land and subsequent environmental pollution.

Conflict of interest:

The authors declare no conflict of interest for this study.

Acknowledgments

The authors are thankful to the Bangabandhu Sheikh Mujibur Rahman Science and Technology University (BSMRSTU), Gopalganj-8100, Bangladesh for their support.

References

Adam, F., Appaturi, J.N., Khanam, Z., Thankappan, R., Nawi, M.A.M., 2013. Utilization of tin and titanium incorporated rice husk silica nanocomposite as photocatalyst and adsorbent for the removal of methylene blue in aqueous medium. Applied Surface Science 264, 718-726.

Ag, E.S., Na, B., Garamon, S., 2018. Adsorption of Heavy Metal Ions from Aqueous Solutions onto Rice Husk Ash Low Cost Adsorbent. Journal of Environmental & Analytical Toxicology 8(1), 1-5.

Agbovi, H.K., Wilson, L.D., 2021. 1 - Adsorption processes in biopolymer systems: fundamentals to practical applications, in: Kalia, S. (Ed.) Natural Polymers-Based Green Adsorbents for Water Treatment. Elsevier, pp. 1-51.

Alam, M.M., Hossain, M.A., Hossain, M.D., Johir, M.A.H., Hossen, J., Rahman, M.S., Zhou, J.L., Hasan, A.T.M.K., Karmakar, A.K., Ahmed, M.B., 2020. The Potentiality of Rice Husk-Derived Activated Carbon: From Synthesis to Application. Processes 8(2).

Alexander, G.B., Heston, W.M., Iler, R.K., 1954. The Solubility of Amorphous Silica in Water. The Journal of Physical Chemistry 58(6), 453-455.

Alver, E., Metin, A.Ü., Brouers, F., 2020. Methylene blue adsorption on magnetic alginate/rice husk bio-composite. International Journal of Biological Macromolecules 154, 104-113.

Azat, S., Korobeinyk, A.V., Moustakas, K., Inglezakis, V.J., 2019. Sustainable production of pure silica from rice husk waste in Kazakhstan. Journal of Cleaner Production 217, 352-359.

Azevedo, A.C.N., Vaz, M.G., Gomes, R.F., Pereira, A.G.B., Fajardo, A.R., Rodrigues, F.H.A., 2017. Starch/rice husk ash based superabsorbent composite: high methylene blue removal efficiency. Iranian Polymer Journal 26(2), 93-105.

Bakar, R.A., Yahya, R., Gan, S.N., 2016. Production of High Purity Amorphous Silica from Rice Husk. Procedia Chemistry 19, 189-195.

448 Bakdash, R.S., Aljundi, I.H., Basheer, C., Abdulazeez, I., 2020. Rice husk derived Aminated Silica
449 for the efficient adsorption of different gases. Scientific Reports 10(1), 19526.
450 Beidaghy Dizaji, H., Zeng, T., Enke, D., 2021. Mitigation of Ash-Melting Behavior during
451 Combustion of Silica-Rich Biomass Assortmentst to Enhance Porosity of Biogenic Silica,
452 European Biomass Conference and Exhibition Proceedings. pp. 713-718.
453 Beidaghy Dizaji, H., Zeng, T., Enke, D., 2022a. New fuel indexes to predict ash behavior for
454 biogenic silica production. Fuel 310, 122345.
455 Beidaghy Dizaji, H., Zeng, T., Hartmann, I., Enke, D., Schliermann, T., Lenz, V., Bidabadi, M.,
456 2019. Generation of High Quality Biogenic Silica by Combustion of Rice Husk and Rice
457 Straw Combined with Pre- and Post-Treatment Strategies—A Review. Applied Sciences 9(6).
458 Beidaghy Dizaji, H., Zeng, T., Hölzig, H., Bauer, J., Klöß, G., Enke, D., 2022b. Ash
459 transformation mechanism during combustion of rice husk and rice straw. Fuel 307, 121768.
460 BRRI, 2021. Bangladesh Rice Knowledge Bank. http://www.knowledgebank-
461 brri.org/riceinban.php. (Accessed June 2021)
462 Chandrasekhar, S., Pramada, P.N., 2006. Rice husk ash as an adsorbent for methylene blue—effect
463 of ashing temperature. Adsorption 12(1), 27.
464 Chen, X.-G., Lv, S.-S., Liu, S.-T., Zhang, P.-P., Zhang, A.-B., Sun, J., Ye, Y., 2012. Adsorption
465 of Methylene Blue by Rice Hull Ash. Separation Science and Technology 47(1), 147-156.
466 Chun, J., Lee, J.H., 2020. Recent Progress on the Development of Engineered Silica Particles
467 Derived from Rice Husk. Sustainability 12(24).
468 Chun, J., Mo Gu, Y., Hwang, J., Oh, K.K., Lee, J.H., 2020. Synthesis of ordered mesoporous silica
469 with various pore structures using high-purity silica extracted from rice husk. Journal of
470 Industrial and Engineering Chemistry 81, 135-143.

Costa, J.A.S., Paranhos, C.M., 2018. Systematic evaluation of amorphous silica production from rice husk ashes. Journal of Cleaner Production 192, 688-697.

Costa, J.A.S., Paranhos, C.M., 2019. Evaluation of rice husk ash in adsorption of Remazol Red dye from aqueous media. SN Applied Sciences 1(5), 397.

Dutta Gupta, A., Bhadauria, V., Singh, H., 2021. Silica derived from rice husk ash and loaded with iron oxide for As(III) adsorption from water: experimental and modelling studies. International Journal of Environmental Analytical Chemistry, 1-24.

Ejiofor, O.S., Okoro, P.A., Ogbuefi, U.C., Nnabuike, C.V., Okedu, K.E., 2020. Off-grid electricity generation in Nigeria based on rice husk gasification technology. Cleaner Engineering and Technology 1, 100009.

He, S., Chen, G., Xiao, H., Shi, G., Ruan, C., Ma, Y., Dai, H., Yuan, B., Chen, X., Yang, X., 2021. Facile preparation of N-doped activated carbon produced from rice husk for CO2 capture. Journal of Colloid and Interface Science 582, 90-101.

Hongo, T., Moriura, M., Hatada, Y., Abiko, H., 2021. Simultaneous Methylene Blue Adsorption and pH Neutralization of Contaminated Water by Rice Husk Ash. ACS Omega 6(33), 21604-21612.

Hossain, S.K.S., Mathur, L., Singh, P., Majhi, M.R., 2017. Preparation of forsterite refractory using highly abundant amorphous rice husk silica for thermal insulation. Journal of Asian Ceramic Societies 5(2), 82-87.

Jung, H.J., Kwak, H., Chun, J., Oh, K.K., 2021. Alkaline Fractionation and Subsequent Production of Nano-Structured Silica and Cellulose Nano-Fibrils for the Comprehensive Utilization of Rice Husk. Sustainability 13(4).

493 Kalapathy, U., Proctor, A., Shultz, J., 2000. A simple method for production of pure silica from
494 rice hull ash. Bioresource Technology 73(3), 257-262.
495 Karthigairajan, M., Nagarajan, P.K., Raviraja Malarvannan, R., Ramesh Bapu, B.R.,
496 Jayabalakrishnan, D., Maridurai, T., Shanmuganathan, V.K., 2021. Effect of Silane-Treated
497 Rice Husk Derived Biosilica on Visco-Elastic, Thermal Conductivity and Hydrophobicity
498 Behavior of Epoxy Biocomposite Coating for Air-Duct Application. Silicon 13(12), 4421-
499 4430.
500 Lakshmi, U.R., Srivastava, V.C., Mall, I.D., Lataye, D.H., 2009. Rice husk ash as an effective
501 adsorbent: Evaluation of adsorptive characteristics for Indigo Carmine dye. Journal of
502 Environmental Management 90(2), 710-720.
503 Ma, X., Zhou, B., Gao, W., Qu, Y., Wang, L., Wang, Z., Zhu, Y., 2012. A recyclable method for
504 production of pure silica from rice hull ash. Powder Technology 217, 497-501.
505 Mane, V.S., Deo Mall, I., Chandra Srivastava, V., 2007. Kinetic and equilibrium isotherm studies
506 for the adsorptive removal of Brilliant Green dye from aqueous solution by rice husk ash.
507 Journal of Environmental Management 84(4), 390-400.
508 Me, N., Bee Ling, T., 2016. By-products of Rice Processing: An Overview of Health Benefits and
509 Applications. Rice Research: Open Access 4(1), 1-11.
510 Meléndez-Ortiz, H.I., Perera-Mercado, Y., Mercado-Silva, J.A., Olivares-Maldonado, Y.,
511 Castruita, G., García-Cerda, L.A., 2014. Functionalization with amine-containing
512 organosilane of mesoporous silica MCM-41 and MCM-48 obtained at room temperature.
513 Ceramics International 40(7, Part A), 9701-9707.
514 Moeinian, K., Mehdinia, S.M., 2019. Removing Methylene Blue from Aqueous Solutions Using
515 Rice Husk Silica Adsorbent. Pol. J. Environ. Stud. 28(4), 2281-2287.

Mohamed, F.M., Alfalous, K.A., 2020. The effectiveness of activated silica derived from rice husk in coagulation process compared with inorganic coagulants for wastewater treatment. The Egyptian Journal of Aquatic Research 46(2), 131-136.

Mor, S., Chhoden, K., Ravindra, K., 2016. Application of agro-waste rice husk ash for the removal of phosphate from the wastewater. Journal of Cleaner Production 129, 673-680.

Niculescu, V.-C., Raboaca, M.S., 2021. Efficient Rice-Husk-Derived Silica Nanocatalysts for Organic Dye Removal from Water. Catalysts 11(7).

Park, J.Y., Gu, Y.M., Park, S.Y., Hwang, E.T., Sang, B.-I., Chun, J., Lee, J.H., 2021. Two-Stage Continuous Process for the Extraction of Silica from Rice Husk Using Attrition Ball Milling and Alkaline Leaching Methods. Sustainability 13(13), 7350.

Peres, E.C., Slaviero, J.C., Cunha, A.M., Hosseini–Bandegharaei, A., Dotto, G.L., 2018. Microwave synthesis of silica nanoparticles and its application for methylene blue adsorption. Journal of Environmental Chemical Engineering 6(1), 649-659.

Post, P., Wurlitzer, L., Maus-Friedrichs, W., Weber, A.P., 2018. Characterization and Applications of Nanoparticles Modified in-Flight with Silica or Silica-Organic Coatings. Nanomaterials (Basel, Switzerland) 8(7).

Prempeh, C.O., Formann, S., Schliermann, T., Dizaji, H.B., Nelles, M., 2021. Extraction and Characterization of Biogenic Silica Obtained from Selected Agro-Waste in Africa. Applied Sciences 11(21).

Sadeghi Afjeh, M., Bagheri Marandi, G., Zohuriaan-Mehr, M.J., 2020. Nitrate removal from aqueous solutions by adsorption onto hydrogel-rice husk biochar composite. Water Environment Research 92(6), 934-947.

Sankar, S., Sharma, S.K., Kaur, N., Lee, B., Kim, D.Y., Lee, S., Jung, H., 2016. Biogenerated silica nanoparticles synthesized from sticky, red, and brown rice husk ashes by a chemical method. Ceramics International 42(4), 4875-4885.

Schliermann, T., I. Hartmann, H. Beidaghy Dizaji, T. Zeng, D. Schneider, S. Wassersleben, D. Enke, T. Jobst, A. Lange, Roelofs, F., 2018. High quality biogenic silica from combined energetic and material utilization of agricultural residues, Proceedings of the 7th International Symposium of Energy from Biomass and Waste. Venice, Italy, pp. 15-18.

Sembiring, S., Simanjuntak, W., Situmeang, R., Riyanto, A., Sebayang, K., 2016. Preparation of refractory cordierite using amorphous rice husk silica for thermal insulation purposes. Ceramics International 42(7), 8431-8437.

Sharma, P., Kaur, R., Baskar, C., Chung, W.-J., 2010. Removal of methylene blue from aqueous waste using rice husk and rice husk ash. Desalination 259(1), 249-257.

Shen, Y., 2017. Rice husk silica derived nanomaterials for sustainable applications. Renewable and Sustainable Energy Reviews 80, 453-466.

Silva, L.A., Santos, I.F.S.d., Machado, G.d.O., Tiago Filho, G.L., Barros, R.M., 2021. Rice husk energy production in Brazil: An economic and energy extensive analysis. Journal of Cleaner Production 290, 125188.

Singh, G., Dizaji, H.B., Puttuswamy, H., Sharma, S., 2022. Biogenic Nanosilica Synthesis Employing Agro-Waste Rice Straw and Its Application Study in Photocatalytic Degradation of Cationic Dye. Sustainability 14(1).

Sivalingam, S., Sen, S., 2020. Rice husk ash derived nanocrystalline ZSM-5 for highly efficient removal of a toxic textile dye. Journal of Materials Research and Technology 9(6), 14853-14864.

561 Sobrosa, F.Z., Stochero, N.P., Marangon, E., Tier, M.D., 2017. Development of refractory
562 ceramics from residual silica derived from rice husk ash. Ceramics International 43(9), 7142-
563 7146.
564 Soltani, N., Bahrami, A., Pech-Canul, M.I., González, L.A., 2015. Review on the physicochemical
565 treatments of rice husk for production of advanced materials. Chemical Engineering Journal
566 264, 899-935.
567 Steven, S., Restiawaty, E., Pasymi, P., Bindar, Y., 2021. An appropriate acid leaching sequence in
568 rice husk ash extraction to enhance the produced green silica quality for sustainable industrial
569 silica gel purpose. Journal of the Taiwan Institute of Chemical Engineers 122, 51-57.
570 Suzaimi, N.D., Goh, P.S., Malek, N.A.N.N., Lim, J.W., Ismail, A.F., 2020. Enhancing the
571 performance of porous rice husk silica through branched polyethyleneimine grafting for
572 phosphate adsorption. Arabian Journal of Chemistry 13(8), 6682-6695.
573 Umeda, J., Kondoh, K., 2010. High-purification of amorphous silica originated from rice husks
574 by combination of polysaccharide hydrolysis and metallic impurities removal. Industrial
575 Crops and Products 32(3), 539-544.
576 Van Hoed, V., Depaemelaere, G., Ayala, J.V., Santiwattana, P., Verhe, R., De Greyt, W., 2006.
577 Influence of chemical refining on the major and minor components of rice brain oil. Journal
578 of the American Oil Chemists' Society 83(4), 315-321.
579 Wazir, A.H., Wazir, I.U., Wazir, A.M., 2020. Preparation and characterization of rice husk based
580 physical activated carbon. Energy Sources, Part A: Recovery, Utilization, and Environmental
581 Effects, 1-11.
582 Widjonarko, D.M., Jumina, J., Kartini, I., Nuryono, N.J.I.J.o.C., 2014. Phosphonate Modified
583 Silica for Adsorption of Co(II), Ni(II), Cu(II), and Zn(II). 14, 143-151.

584 Yan, S., Yin, D., He, F., Cai, J., Schliermann, T., Behrendt, F., 2022. Characteristics of Smoldering
585 on Moist Rice Husk for Silica Production. Sustainability 14(1).
586 Zareei, S.A., Ameri, F., Dorostkar, F., Ahmadi, M., 2017. Rice husk ash as a partial replacement
587 of cement in high strength concrete containing micro silica: Evaluating durability and
588 mechanical properties. Case Studies in Construction Materials 7, 73-81.
589 Zareihassangheshlaghi, A., Beidaghy Dizaji, H., Zeng, T., Huth, P., Ruf, T., Denecke, R., Enke,
590 D., 2020. Behavior of Metal Impurities on Surface and Bulk of Biogenic Silica from Rice
591 Husk Combustion and the Impact on Ash-Melting Tendency. ACS Sustainable Chemistry &
592 Engineering 8(28), 10369-10379.
593
594

All Figures

Total 5 Figures

Figure 1:

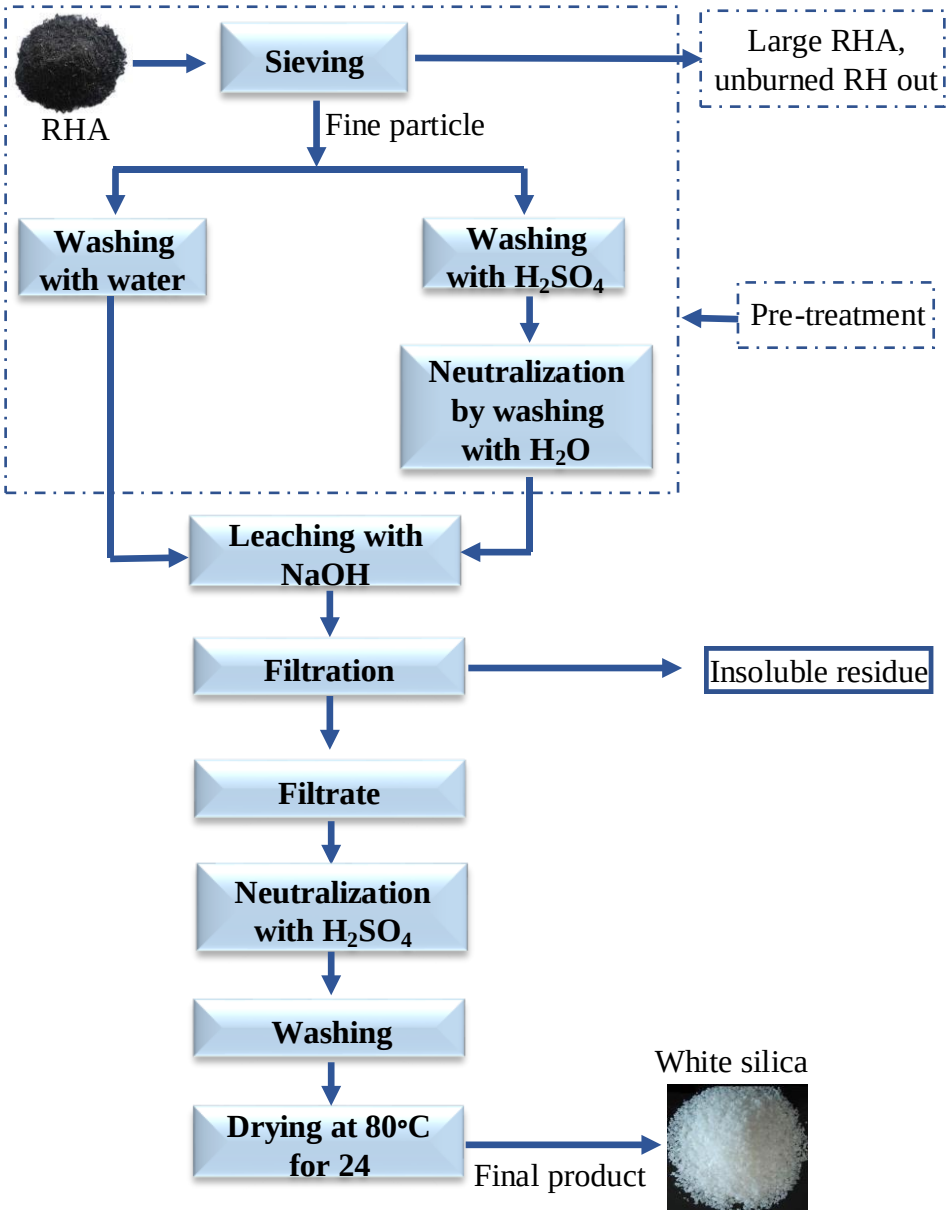

Figure 1: Schematic representation of silica production process.

Figure 2:

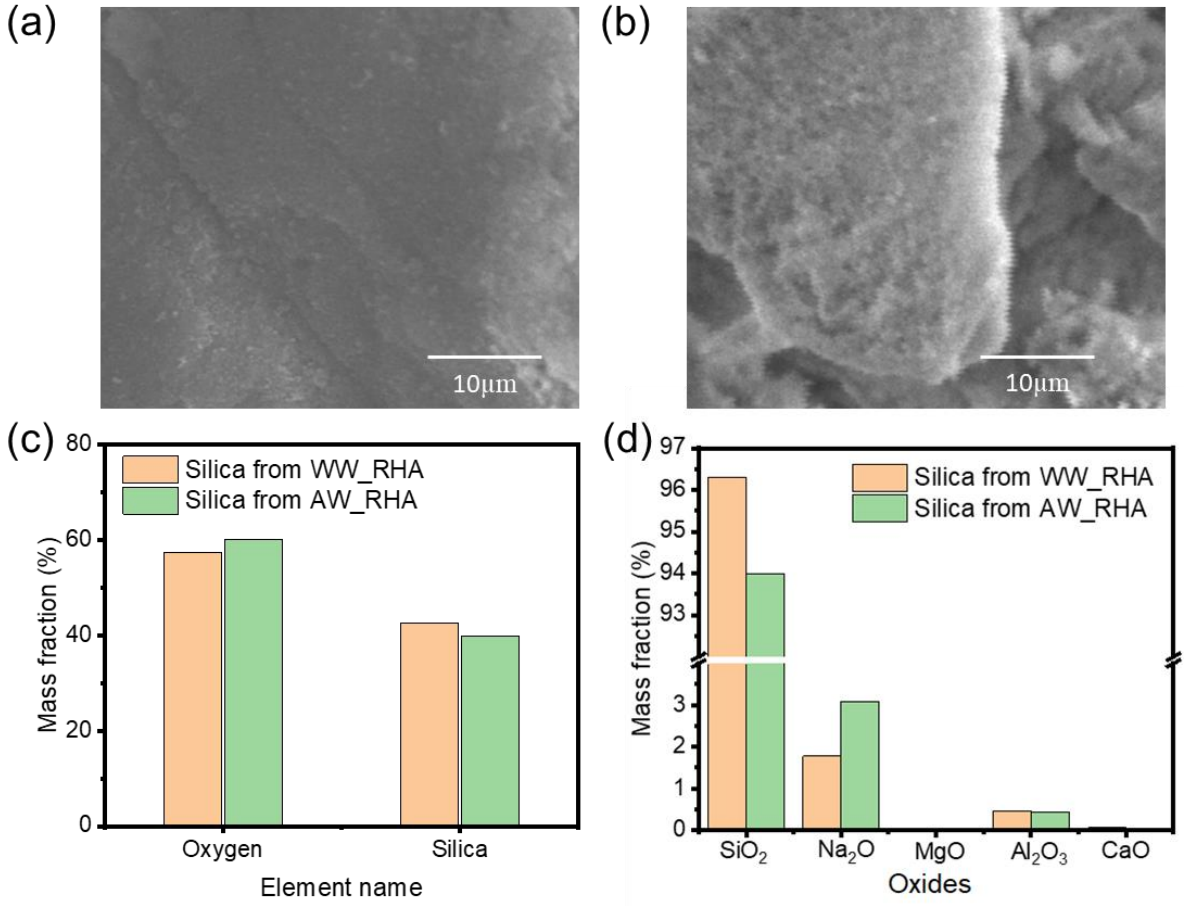

Figure 2: SEM images and EDX analysis of the produced silica with their chemical composition.

Figure 3:

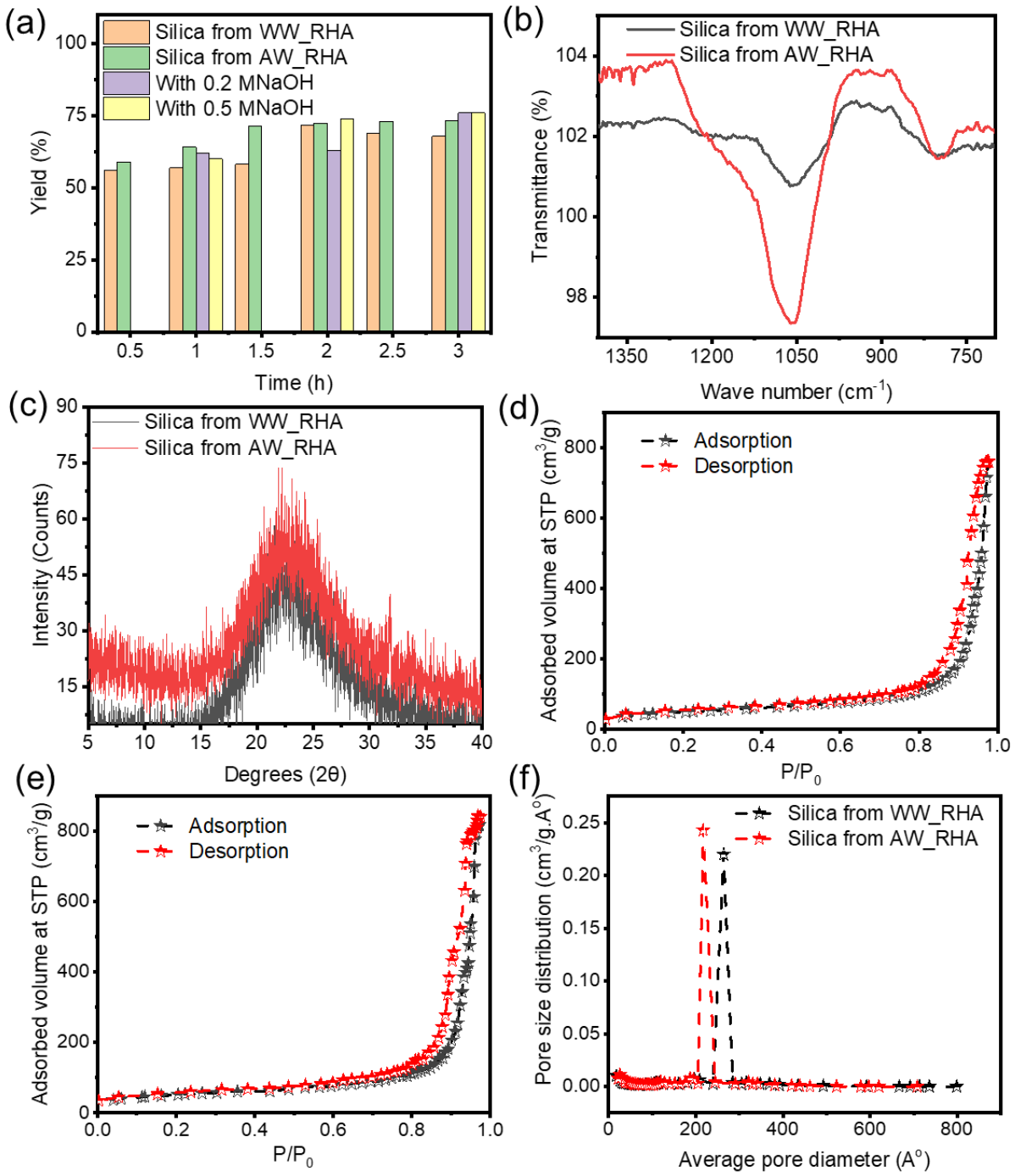

Figure 3: (a) Effect of time on the extraction of silica from RHA. (b) FTIR spectra of produced silica. (c) X-ray diffraction spectra of produced silica. (d) Adsorption-desorption isotherm for silica from water-washed RHA. (e) Adsorption-desorption isotherm for silica from acid-washed

RHA. (f) BJH desorption pore size distribution by volume. In the figure, WW_RHA= Water washed Rice Husk Ash; and AW_RHA= Acid washed Rice Husk Ash.

Figure 4:

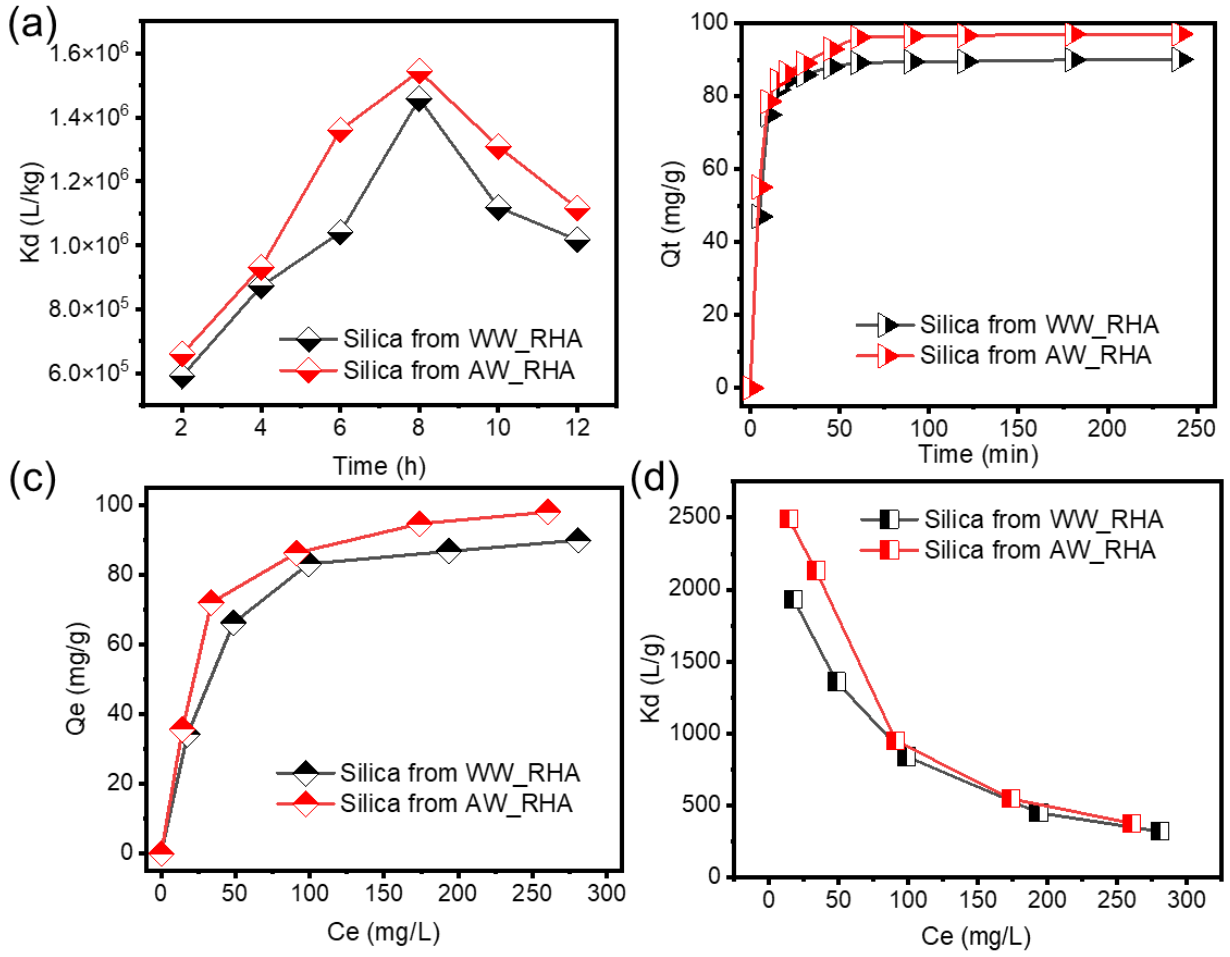

Figure 4: (a) Effect of pH on the distribution coefficient (K_d) for methylene blue removal. (b) Sorption kinetics data with PFO and PSO kinetics model fitting. (c) Sorption isotherm plots and model fitting. (d) Change of K_d values against equilibrium concentrations from isotherm studies.

Figure 5:

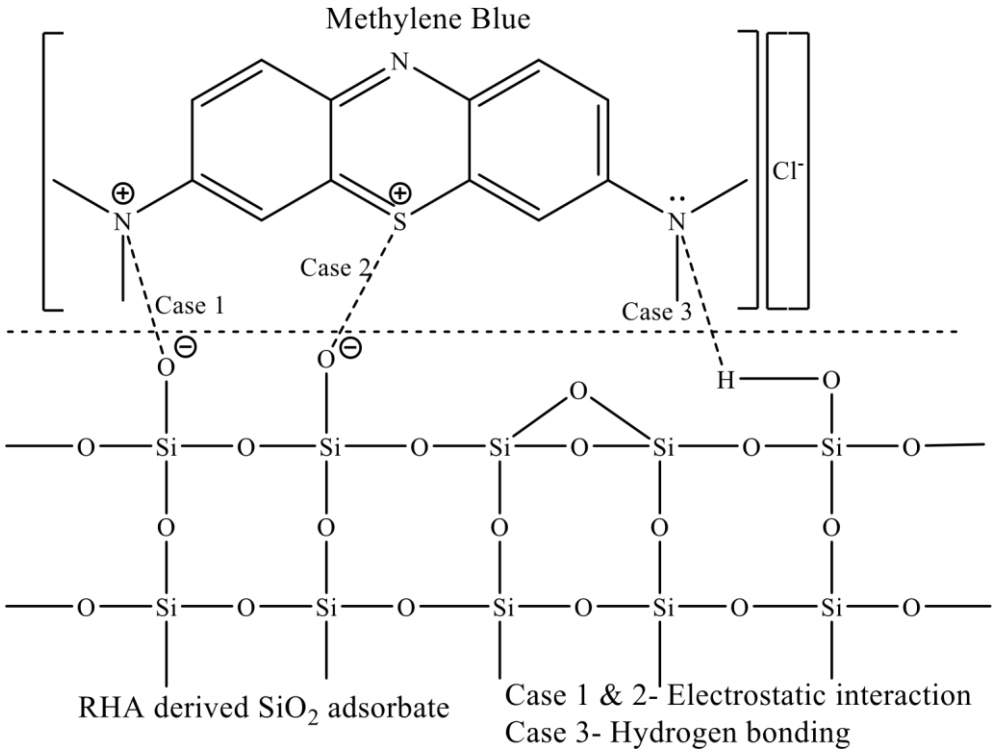

Figure 5: Schematic representation of the proposed mechanism of adsorption of MB on the silica surface.

All Tables

Total 4 Tables

Table 1:

Chemical compositions of silica from different rice husk and rice husk ash samples.

Product	Calcination before or after alkali extraction	Mass percentage (%)					
		SiO_2	Na_2O	MgO	Al_2O_3	CaO	Reference
SiO_2 from water washed RHA	No	96.30	1.78	0.030	0.456	0.062	This study
SiO_2 from H_2SO_4 washed RHA		94.0	3.09	---	0.432	0.025	This study
SiO_2 from unwashed RHA	No	93.00	4.486	<1 ppm	-	0.047	(Kalapathy et al., 2000)
SiO_2 from H_2SO_4 leached RHA	Before	99.08	NA	0.035	0.61	0.05	(Bakar et al., 2016)
SiO_2 from HCl washed RHA	Before	99.58	NA	0.016	0.168	0.043	(Bakar et al., 2016)
SiO_2 from Citric acid-treated RH	Before	98.67	-	-	-	0.11	(Azat et al., 2019)
SiO_2 from HCl acid-treated RH	Before	99.67	-	-	-	0.20	(Azat et al., 2019)
SiO_2 from water-washed RH	After	98.50	0.96	0.01	0.07	0.01	(Park et al., 2021)
SiO_2 from H_2SO_4 washed RH	After	99.80	0.01	0.01	0.04	0.02	(Chun et al., 2020)
SiO_2 from HCl washed RH	Before	96.44	1.38	-	0.18	0.10	(Steven et al., 2021)
SiO_2 from HCl-H_2SO_4 washed RH	Before	97.35	-	-	-	0.27	(Moeinian and Mehdinia, 2019)
SiO_2 from HCl leached Agulhinha RH	Before	98.34	0.32	0.02	1.15	0.02	(Costa and Paranhos, 2018)
SiO_2 from HCl leached Cateto RH	Before	98.24	0.14	0.03	1.31	0.01	(Costa and Paranhos, 2018)

Nano SiO_2 from RHA	After	>98	-	-	-	-	(Jung et al., 2021)
SiO_2 from water-washed RH	Before	93.4	-	0.70	0.21	2.08	(Yan et al., 2022)
SiO_2 from water-washed RH-900	Before	95.73	-	2.38	-	1.88	(Zareihassangheshlaghi et al., 2020)
SiO_2 from Citric acid-treated RH-900	Before	100	-	-	-	-	(Zareihassangheshlaghi et al., 2020)

Table 2:

BET specific surface area of silica produced from RHA.

Product	Calcination before or after alkali extraction	Specific surface area, m^2/g		Total Pore volume, cm^3/g	Average pore diameter (4V/A by BET), Å	Reference
		SP	MP			
SiO_2 from water-washed RHA	No	165.74	177.55	1.1727	277.1612	This work
SiO_2 from H_2SO_4 washed RHA		170.60	182.68	1.0618	233.3785	
SiO_2 from Citric acid-treated RH	Before	625.00		0.770	16.20	(Azat et al., 2019)
SiO_2 from HCl acid-treated RH	Before	150.00		0.750	1840	(Azat et al., 2019)
SiO_2 from H_2SO_4 leached RHA	Before	208.00		0.310	56.80	(Bakar et al., 2016)
SiO_2 from HCl leached RHA	Before	218.00		0.320	55.60	(Bakar et al., 2016)
SiO_2 from water-washed RH	After	1.973		0.004	-	(Park et al., 2021)
SiO_2 from H_2SO_4 washed RH	After	88.00		0.180	-	(Chun et al., 2020)
SiO_2 from HCl leached Agulhinha RH	Before	293.89		0.200	-	(Costa and Paranhos, 2018)
SiO_2 from HCl leached Cateto RH	Before	173.57		0.100	-	(Costa and Paranhos, 2018)
SiO_2 from HNO_3 leached RH	Before	315.00		0.367	73.30	(Adam et al., 2013)
SiO_2 from HCl leached RHA	Before	400.69		-	-	(Steven et al., 2021)
SiO_2 from HCl-H_2SO_4 washed RH	Before	226.30		-	-	(Moeinian and Mehdinia, 2019)
Nano SiO_2 from HCl leached RH	Before	71.97		0.2005	84.40	(Peres et al., 2018)

Nano SiO_2 from water-washed RHA	Before	226.811	1.144	-	(Singh et al., 2022)
Nano SiO_2 from RHA	After	328	0.61	-	(Jung et al., 2021)
SiO_2 from water-washed RH	Before	164.9	-	-	(Yan et al., 2022)
SiO_2 from water-washed RH-900	Before	77	0.16	-	(Zareihassanghes hlaghi et al., 2020)
SiO_2 from Citric acid-treated RH-900	Before	139	0.19	-	(Zareihassanghes hlaghi et al., 2020)

Table 3:

PFO and PSO kinetics data for MB adsorption on RHA.

Adsorbent	Pseudo first order			Pseudo second order			Reference
	Q_e	K_1	R^2	Q_e	K_2	R^2	
SiO_2 from water-washed RHA	90.19	0.151	0.997	95.48	0.003	0.976	This work
SiO_2 from H_2SO_4 washed RHA	96.89	0.166	0.989	102.49	0.003	0.995	This work
Nano SiO_2 from HCl leached RH	118.30	1.270	0.903	124.80	0.015	0.946	(Peres et al., 2018)
RHA at 450℃ in air atmosphere	48.04	-	0.911	48.10	0.069	1.000	(Chen et al., 2012)
RHA at 750℃ in a nitrogen atmosphere	44.99	-	0.891	45.91	0.005	0.999	(Chen et al., 2012)
Kerala RHAed at 500℃	-	-	0.926	-	-	0.999	(Hongo et al., 2021)
Andhra Pradesh RHAed at 500℃	-	-	0.636	-	-	0.999	(Hongo et al., 2021)

Table 4:

Adsorption isotherm data for MB removal.

Adsorbent	Langmuir isotherm parameter			Freundlich isotherm parameter			References
	Q_{max}	K_L	R^2	K_F	1/n	R^2	
SiO_2 from water-washed RHA	107.73	0.045	0.984	24.815	0.2578	0.937	This work
SiO_2 from H_2SO_4 washed RHA	101.83	0.034	0.990	21.043	0.2697	0.938	This work
Nano SiO_2 from HCl leached RH	250.20	0.009	0.994	11.02	0.496	0.998	(Peres et al., 2018)
RHA at 450℃ in air atmosphere	50.51	0.242	0.993	10.904	0.367	0.864	(Chen et al., 2012)
RHA at 750℃ in a nitrogen atmosphere	46.30	0.469	0.999	13.237	0.310	0.943	(Chen et al., 2012)
RHA from the power plant	3.51	1.210	0.999	1.690	0.281	0.864	(Hongo et al., 2021)
Kerala RHAed at 500 ℃	689.66	0.360	0.929	501.65	0.76	0.999	(Chandrasekhar and Pramada, 2006)
Andhra Pradesh RHAed at 500℃	263.16	0.020	1.000	122.78	0.89	0.952	(Chandrasekhar and Pramada, 2006)
SiO_2 from HCl-H_2SO_4 washed RH	103.11	4.400	0.996	20.30	0.621	0.983	(Moeinian and Mehdinia, 2019)

Declaration of Interest Statement

Energy Efficient Extraction of Silica from Rice Husk Ash as Adsorbent for Dye Removal

Jahid Bin Haider[a], Md. Irfanul Haque[a], Mozammel Hoque[b], Md. Mosaddek Hossen[a], M. Mottakin[a], Md. Abdul Khaleq[a], MAH Johir[c], John L. Zhou[c], Mohammad Boshir Ahmedc[c, d*], Masoumeh Zargar[e].

The authors declare no conflict of interest.